

# Effects of Multi-Charge on Aerosol Hygroscopicity Measurement by HTDMA

Chuanyang Shen<sup>1</sup>, Gang Zhao<sup>1,2</sup>, Chunsheng Zhao<sup>1</sup>

<sup>1</sup>Department of Atmospheric and Oceanic Sciences, School of Physics, Peking University, Beijing 100871, China

5 <sup>2</sup>College of Environmental Sciences and Engineering, Peking University, Beijing 100871, China

*Correspondence to:* Chunsheng Zhao (zcs@pku.edu.cn)

**Abstract.** The Humidified Tandem Differential Mobility Analyzer (HTDMA) is widely used to obtain submicron particles' hygroscopic properties. Aerosol size-resolved hygroscopicity parameter  $\kappa$  measured by HTDMA will be influenced by the contribution of multiply charged aerosols, and this effect has seldom been discussed in previous field measurements. Our calculation demonstrates that the number ratio of multiply charged particles is quite considerable for some specific sizes between 100 nm and 300 nm, especially during the polluted episode. The multi charges will further lead to the compression effect of aerosol hygroscopicity in HTDMA measurements. Therefore, we propose a new algorithm to do the multi-charge correction for the size-resolved hygroscopicity  $\kappa$  considering both the compression effect and multi-charge number contribution. The application in field measurements shows that the relatively high hygroscopicity in the accumulation size range will lead to the overestimation of particles' hygroscopicity smaller than 200 nm. The low hygroscopicity in coarse mode particles will lead to the underestimation of accumulation particles between 200 nm and 500 nm. The difference between corrected and measured  $\kappa$  can reach as large as 0.05, highlighting that special attention needs to be paid to the multi-charge effect when the HTDMA is used for the aerosol hygroscopicity measurement.

## 1 Introduction

20 Atmospheric particles can scatter solar radiation and absorb longwave radiation, imposing direct effects on the Earth's radiation balance (Haywood and Boucher, 2000; Bond et al., 2013). They can also indirectly affect the climate through acting as cloud nuclei and modify the cloud optical properties and life cycle (ALBRECHT, 1989; Twomey, 1974; CHARLSON et al., 1992). Both these two effects are closely related to aerosol particle's hygroscopicity, which describes the particle's ability to absorb water at sub or supersaturated conditions (e.g. McFiggans et al., 2006). Aerosol hygroscopicity also plays a vital role in environmental aspects. It has been reported to be an important factor regulating environmental visibility because it can greatly enhance the particle's light scattering efficiency and degrade visibility under relatively high relative humidity (Chen et al., 2012; Xu et al., 2020). It can increase aerosol particle's liquid water content, affect the multiphase chemistry and local photochemistry, and facilitates particle formation and aging processes (Wu et al., 2018; Herrmann et al., 2015; Ervens et al., 2011). For human health, aerosol hygroscopicity directly determines the particle's size, thus modifying the deposition pattern of inhaled particles in the human respiratory tract (Heyder et al., 1986; L ndahl et al., 2007). In general, aerosol particle's hygroscopicity is one of the most important properties when quantifying the particle's climatic and environmental

effects. It's also useful to characterize the particle's detailed chemical information. Therefore, it's necessary to offer a correct and detailed measurement of aerosol hygroscopicity.

Nowadays, many instruments have been used to characterize aerosol particle's hygroscopicity, and HTDMA is one of the most widely used (Swietlicki et al., 2008; Tang et al., 2019; Kreidenweis and Asa-Awuku, 2014). As it can directly give the particle's size distribution after water uptake, it can be employed to obtain both the mixing state and bulk mean hygroscopic properties of ambient aerosol particles. Two Differential Mobility Analyzers (Swietlicki et al., 2008) are used in this technique to quantify the size change of particles under different RH exposure. The measured distribution function (MDF) is skewed and smoothed from the particle's actual growth factor probability density function (GF-PDF). So several inversion algorithms have been developed to inverse the true GF-PDF (Cubison et al., 2005; Gysel et al., 2009; Stolzenburg and McMurry, 2008; Voutilainen et al., 2000). These inversions include the TDMAfit algorithm, the optimal estimation method (OEM), and the TDMAinv algorithm. However, these algorithms are based on the assumption that the particles sampled are dominated by singly charged particles. Under this condition, the forward function can be simplified and data analysis is limited within the size concerned, not influenced by other sizes. If the number fraction of multiply charged particles at the selected dry diameter becomes significant, the measured results will be affected by the contributions from other dry sizes. In this case, appropriate data inversion is quite complicated.

However, in some special cases, the accurate data inversion for multi-charge particles can be achieved when the sampled particles are exclusively doubly or triply charged. Gysel et al. (2009) obtained the kernel functions for multiply charged particles and Duplissy et al. (2008) applied them in the data inversion to retrieve the correct growth factors (GFs). The dry sizes he selected are dominated by doubly or triply charged particles. However, in most field measurements, this assumption is invalid. As far as we are concerned, no previous studies have done the multi-charge correction for atmospheric aerosol particles in the HTDMA measurement. The effect of multi-charge correction on the size-resolved hygroscopicity is also not fully evaluated for atmospheric aerosols.

In this study, we first analyse the number contribution from particles carrying different charges. Then we present the compression effect of multiply charged particle's hygroscopicity in the HTDMA measurement. These two effects were included into the algorithm to do the multi-charge correction for particles' size-resolved hygroscopicity. Then the application and corresponding influences of multi-charge correction on particle's hygroscopicity were discussed.

## **2 Multi-Charge Effects**

### **2.1 Number Contribution from multiply charged particles**

In the DMA sizing process, only particles within a narrow range of electrical mobility ( $Z_p$ ) can transmit through the classifier exit slit and come to the downstream humidification and size distribution measurement system. The electrical mobility is defined as:

$$Z_p = \frac{veC(D_p)}{3\pi\mu D_p} \quad (1)$$

where  $C(D_p)$  is the Cunningham slip correction; the  $e$  is elementary charge; the  $v$  is the number of elementary charges on the particle; the  $\mu$  is the gas viscosity poise and  $D_p$  is the particle's physical diameter. From the equation (1), we can see that with the same electrical mobility, particles can have different combinations of diameters and number of charges, and this is where multi-charge effects come from.

The range that can pass through the DMA is defined as the mobility bandwidth,  $\Delta Z_p$ :

$$\Delta Z_p = \frac{q_a}{q_{sh}} Z_p^* \quad (2)$$

where the  $Z_p^*$  is the set mobility, and the  $q_a$  and  $q_{sh}$  is the aerosol flow rate and sheath air flow rate, respectively. This equation doesn't account for diffusion broadening.

We can calculate the particle charge distribution at each size based on a theoretical model developed by Wiedensohler et al. (1986). Then the particle's probability to pass through a DMA classifier can be determined using the kernel function  $G(D_p^*, x)$ :

$$G(D_p^*, x) = \sum_{v=1}^{\infty} F(x, v) \Omega(x, v, D_p^*) \quad (3)$$

where the  $D_p^*$  is the diameter set in the DMA and  $x$  is the scale parameter;  $F(x, v)$  is the charge distribution of particles that exit from a neutralizer with  $v$  charges at the scale parameter  $x$ .  $\Omega(x, v, D_p^*)$  is the probability of particles to pass through the DMA when the set diameter is  $D_p^*$ . In this study, the maximum value of  $v$  is set as 10.

Therefore, given a particle number size distribution  $n(x)$ , the number of particles that can pass through the DMA with a set diameter of  $D_p^*$  is:

$$N(D_p^*) = \int_0^{\infty} G(D_p^*, x) n(x) dx \quad (4)$$

If the number of particles carrying specific charges is needed, the kernel function in the equation (4) need to be replaced with:

$$G_v(D_p^*, x) = F(x, v) \Omega(x, v, D_p^*) \quad (5)$$

and the corresponding number concentration of particle that can pass through the DMA is:

$$N_v(D_p^*) = \int_0^{\infty} G_v(D_p^*, x) n(x) dx \quad (6)$$

The number ratio of particles carrying different charges can be calculated from  $N_v(D_p^*)/N(D_p^*)$ .

Two aerosol size distribution cases representing a relatively clean period and a polluted period during our field measurement (refer to section 4) are shown in Fig. 1. The corresponding ratio of particles carrying different charges is calculated from the PNSD using the abovementioned DMA electrical mobility and charging theory. The detailed calculation procedures can be referred to in the supplement section 1. During the polluted period when total particle volume concentration is large, an obvious feature in PNSD is that the accumulation mode larger than 100 nm grows very large. The growth of this mode leads to an increase in the proportion of multi-charged particles, especially in the size range of 100-300 nm (electrical mobility

diameter). For example, when we set 100 nm in the first DMA, more than 40% of the selected particles are multiply charged. This ratio is about 30% and 20% for the electrical diameter of 200 nm and 300 nm, respectively. Thus the HTDMA measured size-resolved hygroscopicity will also be influenced by those multiply charged large particles.

## 2.2 Compression effect of Hygroscopicity

In previous studies, Gysel et al. (2009) presented that the center of the kernel function at higher charges is systematically offset toward smaller GFs. An illustration figure (Fig.2) was shown to explain the cause of this compression effect. For electrical mobility diameter of 100 nm, the doubly and triply charged particles are about 151 nm and 196 nm, respectively. When all these three kinds of particles have a true growth factor of 1.6, they will grow to the size of 160 nm, 242 nm, and 314 nm. Since the number of charges they carry remains the same as before, their peak sizes in the second DMA are around 160 nm, 154 nm, and 150 nm. Therefore, the growth factors they display in the HTDMA measurement are 1.6, 1.54 and 1.5, respectively. It can be clearly seen that the growth factor is decreased or compressed. We call this phenomenon as the compression effect of growth factor or hygroscopicity brought by the multi-charge.

In the electrical mobility theory, when we set a diameter  $D_p^*$  in the DMA, the electrical mobility,  $Z_p$ , can be calculated as:

$$Z_p = \frac{eC(D_p^*)}{3\pi\mu D_p^*} \quad (7)$$

Then the physical diameter ( $D_p^v$ ) of particles having the same electrical mobility but with  $v$  charges is:

$$D_p^v = \frac{veC(D_p^*)}{3\pi\mu Z_p} = \frac{C(D_p^v)}{C(D_p^*)} v D_p^* \quad (8)$$

and we define the  $f$  function as:

$$D_p^v = f(D_p^*, v). \quad (9)$$

The  $f$  function describes the physical diameter of multiply charged particles given an electrical mobility diameter. The properties and detailed calculation procedures of  $f$  function can be found in the supplement section 2.

For a particle of size  $D_p^v$  with  $v$  charges, if we assume a true growth factor of  $g_0$ , the particle will grow to the size of  $g_0 D_p^v$ . The virtual growth factor depicted in the DMA is expressed as  $g_{DMA}$ . These parameters will fit into this equation:

$$g_0 D_p^v = f(g_{DMA} D_p^*, v) = g_0 f(D_p^*, v). \quad (10)$$

Given the  $f$  function,  $D_p^*$ , and  $v$ , each  $g_0$  can be substituted into the equation (10) to get a corresponding  $g_{DMA}$ . If  $v = 1$ , namely, particles carrying only one elementary charge, then  $g_{DMA}$  is equal to  $g_0$ . If  $v > 1$ , namely, particles are multiply charged, then the  $g_{DMA}$  will be lower than  $g_0$ . In Fig.2(b), an example is presented with  $D_p^* = 100 \text{ nm}$  and  $v = 2$ . The X-axis is the assumed true growth factor ( $g_0$ ) and the Y-axis is the calculated virtual growth factor depicted in DMA ( $g_{DMA}$ ). Generally, the larger the  $g_0$  is, the greater the difference between  $g_{DMA}$  and  $g_0$  is.

According to Petters and Kreidenweis (2007), aerosol particle's hygroscopic parameter  $\kappa$  can be calculated from the growth factor under a specific RH using  $\kappa$ -kohler theory. As illustrated in Fig.3a, all the data points in Fig.2b can generate

125 corresponding data points in the hygroscopicity space. It is clear that the decreased growth factor will result in a decreased  
 hygroscopicity and the compression effect also increases almost linearly with the particle's hygroscopicity. If we fit these  
 data points with a straight line across the origin, the slope can be considered as the compression factor. Fig.3a is an example  
 for  $D_p^* = 100 \text{ nm}$  and  $\nu = 2$ . For each combination of electrical mobility diameter  $D_p^*$  and number of charges  $\nu$ , we can  
 repeat this calculation and linear fitting process, and obtain the compression factor  $S(D_p^*, \nu)$  for hygroscopicity. The  
 130 algorithm to calculate the compression factor is listed in Fig.4 and the results are summarized in Fig.3b and Table 1.

### 3 Method of Multi-Charge Correction

#### 3.1 Multi-charge correction for size-resolved hygroscopicity

Multi-charge corrections are common when the DMA is used to scan the aerosol sizes, especially in the PNSD  
 135 measurements. The shape of PNSD after multi-charge correction can be significantly different from that of the raw measured  
 one. Therefore, it's necessary to evaluate the effect of multi-charge correction on the size-resolved hygroscopicity obtained  
 by HTDMA. This study developed an algorithm to do the multi-charge correction for the measured values based on the work  
 of Deng et al. (2011) and Zhao et al. (2019)

Our correction is based on the assumption that, for each electrical mobility set at DMA1, the measured mean hygroscopicity  
 140 is contributed by all particles that can pass through the DMA1. All the contributing particles carry the mean hygroscopicity  
 of its physical size. For example, when a particle with a larger dry diameter ( $D_p^y$ ) carrying n charges pass through the DMA1  
 and make a contribution to the MDF, it's hard to tell which hygroscopicity it carries because it has a probability distribution  
 function over hygroscopicity. In our algorithm, this particle is assumed to have a hygroscopicity of the mean value in the size  
 $D_p^y$ . This assumption is statistically right and feasible but may not be true on a single-particle scale.

145 When the scan diameter in the first DMA is set as  $D_p^*$ , the observed mean hygroscopicity  $K^*$  by HTDMA can be expressed  
 as:

$$K^*(D_p^*) = \frac{1}{N(D_p^*)} \int_0^\infty G_s(D_p^*, x) K(x) n(x) dx \quad (11)$$

where  $K(x)$  is the true mean  $\kappa$  for the scale parameter  $x$ ;  $n(x)$  is the true aerosol number size distribution;  $N(D_p^*)$  is the total  
 number concentration of particles that pass through the first DMA. The  $G_s(D_p^*, x)$  is the transformed kernel function  
 150  $G(D_p^*, x)$  of DMA1, which includes the compression effect  $S(D_p^*, \nu)$ .

$$G_s(D_p^*, x) = \sum_{\nu=1}^\infty F(x, \nu) \Omega(x, \nu, D_p^*) S(D_p^*, \nu) \quad (12)$$

$$N(D_p^*) = \int_0^\infty G(D_p^*, x) n(x) dx \quad (13)$$

So the equation (5) can be simplified into the following:

$$K^*(D_p^*) = \int_0^\infty H(D_p^*, x)K(x)dx \quad (14)$$

155 or

$$\mathbf{K}^* = \mathbf{H}\mathbf{K} \quad (15)$$

where the  $K(x)$  or  $\mathbf{K}$  is the true distribution of  $\kappa$  we want to obtain, and  $K^*(D_p^*)$  or  $\mathbf{K}^*$  is the measured  $\kappa$  distribution.

$H(D_p^*, x)$  is:

$$H(D_p^*, x) = \frac{1}{N(D_p^*)}n(x)G^*(D_p^*, x)dx \quad (16)$$

160  $H(D_p^*, x)$  or  $\mathbf{H}$  matrix is the forward function and can be calculated from given information. Given a true  $\kappa$  distribution, we should be able to calculate the measured  $\kappa$  distribution imposed by multi-charge effect. The  $\mathbf{H}$  matrix accounts for the DMA transfer function, the particle charge distribution, compression factors and number distribution of particles over each size parameter. The detailed steps to solve this matrix inverse problem can be found in Zhao et al. (2019)

One hypothetical uncorrected  $\kappa$  distribution  $K^*(D_p^*)$  along with the corresponding multi-charge corrected  $K(x)$  are shown in  
 165 Fig.4. It represents a common case in the ambient environment: relatively low hygroscopicity for ultrafine particles, high hygroscopicity in accumulation mode size and nearly hydrophobic in the coarse mode. Two PNSD are used in the multi-charge correction, representing clean and pollution conditions. It can be seen that large variation of  $\kappa$  over sizes will cause large difference between pre- and post-corrected  $\kappa$  distribution, especially when the large variation exists in the singly, doubly and triply charged particle sizes. For example, the difference between measured and corrected  $\kappa$  reach a peak in 150  
 170 nm and 350 nm. For electrical mobility size of 150 nm, the corresponding doubly and triply charged particles are around 235 nm and 314 nm. These three sizes are located in the area where  $\kappa$  increases steeply. Similarly, for electrical mobility size of 350 nm, the corresponding doubly and triply charged particles are about 605 nm and 852 nm. These three sizes are also located in the area where  $\kappa$  drops greatly. Another point that can be seen from Fig. 4 is that an increasing trend of  $\kappa$  will cause the measured  $\kappa$  overestimated and a decreasing trend of  $\kappa$  will cause the measured  $\kappa$  underestimated.

175

### 3.2 Multi-charge correction for mixing state

Except for the size-resolved mean hygroscopicity, the key information that can be obtained from the HTDMA also includes the mixing state and the detailed shape of GF-PDF or  $\kappa$ -PDF. The correction of GF-PDF or  $\kappa$ -PDF involves the inversion of two-dimensional vectors, which is too complicated for this study. But the mixing state can be simply represented by the  
 180 particle number fraction in different GF ranges. Here, we can use the number fraction of Less-Hygroscopic particles as an example.

The correction for mixing state is similar in general to the correction for mean hygroscopicity, but differ in some minor aspects. When the scan diameter in DMA is set as  $D_p^*$ , the observed number fraction of less-hygroscopic particles by HTDMA can be expressed as:

$$185 \quad M^*(D_p^*) = \frac{1}{N(D_p^*)} \int_0^\infty G_s(D_p^*, x) M(x) n(x) dx \quad (17)$$

where the  $M^*(D_p^*)$  is the measured number fraction of LH group particles at the DMA selected diameter  $D_p^*$ ; the  $M(x)$  represents the true number fraction at scale parameter  $x$ .

$$G_s(D_p^*, x) = \sum_{v=1}^\infty F(x, v) \Omega(x, v, D_p^*) S_M(D_p^*, v) \quad (18)$$

$$N(D_p^*) = \int_0^\infty G(D_p^*, x) n(x) dx \quad (19)$$

190 where the  $S_M(D_p^*, v)$  represents the correction factor caused by the compression effect. This factor varies with different GF-probability distribution function (GF-PDF) and cannot be simplified into a constant. If we assume that the compression effect on the LH number ratio can be neglected, then this parameter is 1 and the equation can be simplified into:

$$M^*(D_p^*) = \int_0^\infty H(D_p^*, x) M(x) \quad (20)$$

or

$$195 \quad \mathbf{M}^* = \mathbf{H}\mathbf{M} \quad (21)$$

where  $H(D_p^*, x)$  is:

$$H(D_p^*, x) = \frac{1}{N(D_p^*)} n(x) G(D_p^*, x) dx \quad (22)$$

The  $H(D_p^*, x)$  or the  $\mathbf{H}$  matrix can also be calculated from given information. One hypothetical measured  $M^*(D_p^*)$  distributions along with the corresponding multi-charge corrected  $M(x)$  distributions are also shown in Fig.5.

200

#### 4 Application in field measurements

During the winter of 2019, a comprehensive aerosol field measurement focusing on hygroscopicity properties over a size range of 50-600 nm was conducted at a Beijing urban site. The measurement was conducted on the rooftop of a six-floor building in the campus of Peking University. It shares the same location with the AERONET station of BEIJING\_PKU (39°  
205 59' N, 116°18' E). The sampling site is in the northwest of Beijing, surrounded by schools, residential buildings, and shopping centers.

During the measurement, an HTDMA instrument was employed to measure hygroscopic growth factors of particles with dry diameters of 50, 100, 200, 300, 400, 500, and 600 nm at 85% RH. Before the aerosol sampling, a PM10 impactor was used to remove aerosol particles with aerodynamic diameters larger than 10  $\mu\text{m}$ . Then a dryer was used to decrease the RH to less  
210 than 30%. Next, the dried poly-disperse particles were guided into a splitter with different instruments located downstream. These instruments include the HTDMA and a BMI scanning electrical mobility sizer (BMI SEMS, Model 2100). In both these two measurement systems, aerosol particles were firstly charged by a soft X-ray neutralizer (TSI, Model 3088) and those negatively charged particles were selected by the DMA. For the HTDMA, the ratio of sample to sheath in the first DMA is 0.75/4. To calibrate the measurement system, ammonium sulfate particles were tested to compare with the

215 theoretical values. The calibration includes both the dry test and RH test. For the best working performance, the room was  
air-conditioned at 25°C and circulated all the time. Particle number size distributions (PNSD) were given by the SEMS with  
a size range of 10-1000 nm.

To evaluate the effects of multiply charged particles on the size-resolved hygroscopicity, we choose two weeks'  
measurement data to do the multi charge correction. The particle number size distribution and measured size-resolved  
220 hygroscopicity  $\kappa$  are shown in Fig. 6. For better comparison, we also present the size-resolved difference between measured  
and corrected hygroscopicity data. What's to be noted is that, since the upper limit of hygroscopicity measurement is 600  
nm, the hygroscopicity in the higher size range is assumed to decrease linearly to 0 at 1  $\mu\text{m}$ . Here we presume the  
hygroscopicity for coarse mode particles is 0. For particles larger than 1  $\mu\text{m}$ , the number concentration is also assumed to  
decrease linearly to 0 at 1.2  $\mu\text{m}$  in the multi-charge correction.

225 Generally, for particles less than 200 nm, the particle's hygroscopicity will be overestimated. For particles larger than 200  
nm, the particle's hygroscopicity will be underestimated. From Fig. 6(b), we can see that in the urban environment, the  
hygroscopicity often peaks at the size range of 200-400 nm. The relatively high hygroscopicity in this size range will be  
mixed into the smaller size in the HTDMA measurement, leading to a false increase of measured  $\kappa$ . Similarly, most of the  
ambient particles have a relatively lower hygroscopicity in the upper size. When they carry multiple charges and sneak into  
230 to the lower accumulation size set by the DMA, the hygroscopicity in the target size region will be lowered.

The overall difference between corrected and measured size-resolved  $\kappa$  mostly lie within 0.05. For the electrical mobility  
size that affected most by multi-charge particles, e.g. 100 nm, the doubly or triply charged particles correspond to 151 nm  
and 196 nm. These three sizes normally share similar hygroscopicity, which leads to a small effect on the measured  $\kappa$ .  
However, when there exists a large variation of hygroscopicity in these three sizes, the multi-charge correction in this size  
235 will be necessary. For particles larger than 300 nm, the multi-charge effect is mostly contributed by particles larger than 500  
nm. Few field observations on hygroscopicity have covered this size range, which brought large uncertainty to the multi-  
charge correction. From our measurement, the variation of hygroscopicity in this size range is relatively large, depending on  
different pollution conditions (Shen et al., 2020). On average, the hygroscopicity of particles above 500 nm is lower than  
other accumulation sizes. Because of the assumption of few particles above 1  $\mu\text{m}$ , the multi-charge effect on the size above  
240 500 nm is fairly small. In practice, this can be achieved by installing an impactor before the inlet of the first DMA.

## 5 Conclusion

The HTDMA instrument has been extensively used in numerous field measurements to obtain the hygroscopic properties of  
submicron particles. Aerosol particles sampled by the DMA are quasi-monodisperse with different charges and different  
diameters. Thus, size-resolved hygroscopicity measured by DMA will be influenced by the contribution of multiply charged  
aerosols. In the hygroscopicity measurement by HTDMA, this effect has seldom been discussed in previous field  
245 measurements.



In this study, we first demonstrate that the multi-charge not only influence the hygroscopicity measurement through the number contribution, but also through the compression effect. On one hand, the number fraction of multiply charged particles is quite considerable, especially under polluted conditions. Results show that there can be 30% to 40% of selected particles are mistaken from large multiply charged particles in the polluted period. On the other hand, the growth factor or hygroscopicity measured by the HTDMA can be smaller than the true value for multiply charged particles, which is also called the multi-charge compression effect. This effect can be quantified as a compression factor using the electrical mobility theory. The compression factor reaches its peak around the size of 200 nm and increases with the number of charges the particle carries.

We propose an algorithm to do the multi-charge correction for the size-resolved hygroscopicity  $\kappa$  and mixing state. The algorithm is based on the principle of SMPS multi-charge correction and the knowledge of aerosol PNSD is required. The key in this algorithm is to obtain the forward function and to solve the inverse problem.

The proposed multi-charge correction is applied in a field measurement to evaluate the multi-charge effects. The relatively high hygroscopicity in accumulation size range will lead to overestimation of the particle's hygroscopicity smaller than 200 nm. The low hygroscopicity in coarse mode particles will lead to the underestimation of accumulation particles. The difference between measured and corrected  $\kappa$  can reach as large as 0.05.

The measured hygroscopicity between 200 nm and 400 nm is influenced by multiply charged particles larger than 400 nm, indicating that the hygroscopic measurement above 400 nm is necessary if correct hygroscopic properties want to be obtained for accumulation mode particles. For particles larger than 400 nm, the multi-charge effect can be removed by installing an impactor with cutting size around 1  $\mu\text{m}$  or even lower. In the future hygroscopicity measurements, our studies highlight that special attention should be paid to the multi-charge effects, and multi-charge correction should be done if accurate size-resolved hygroscopicity needs to be obtained.

**Competing interests.** The authors declare that they have no conflict of interest.

**Data availability.** The data used in this study is available when requesting the authors.

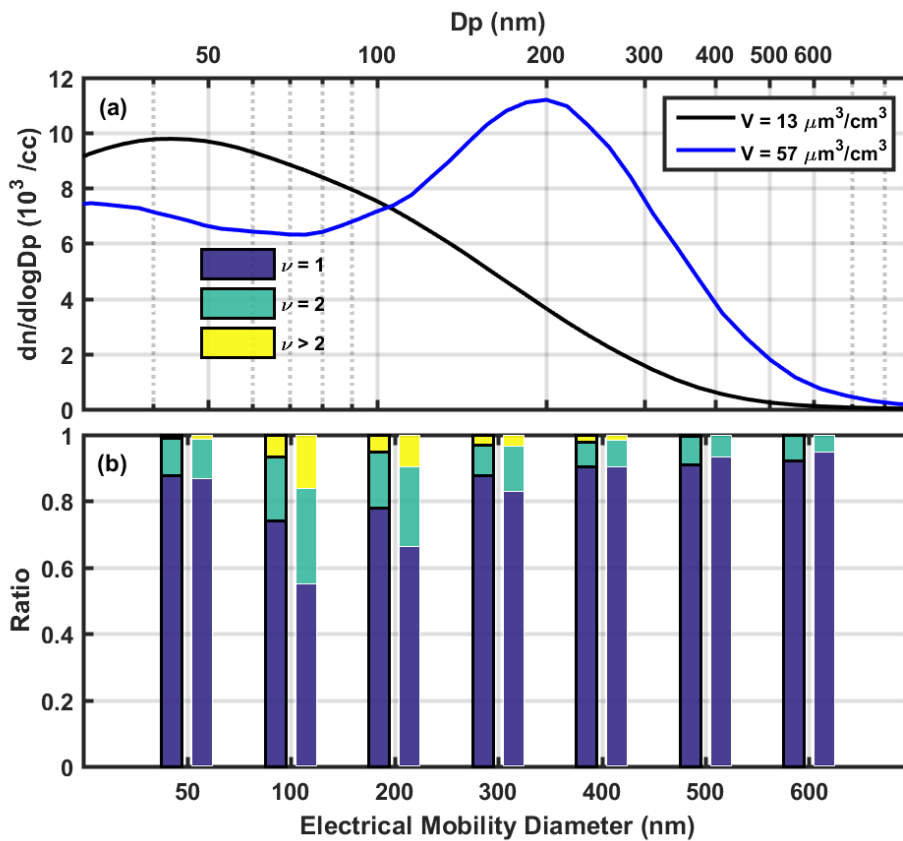
**Author contributions.** Chuanyang Shen, Gang Zhao and Chunsheng Zhao discussed the results; Chuanyang Shen wrote the manuscript.

**Acknowledgements.** This work is supported by the National Natural Science Foundation of China (41590872).

275

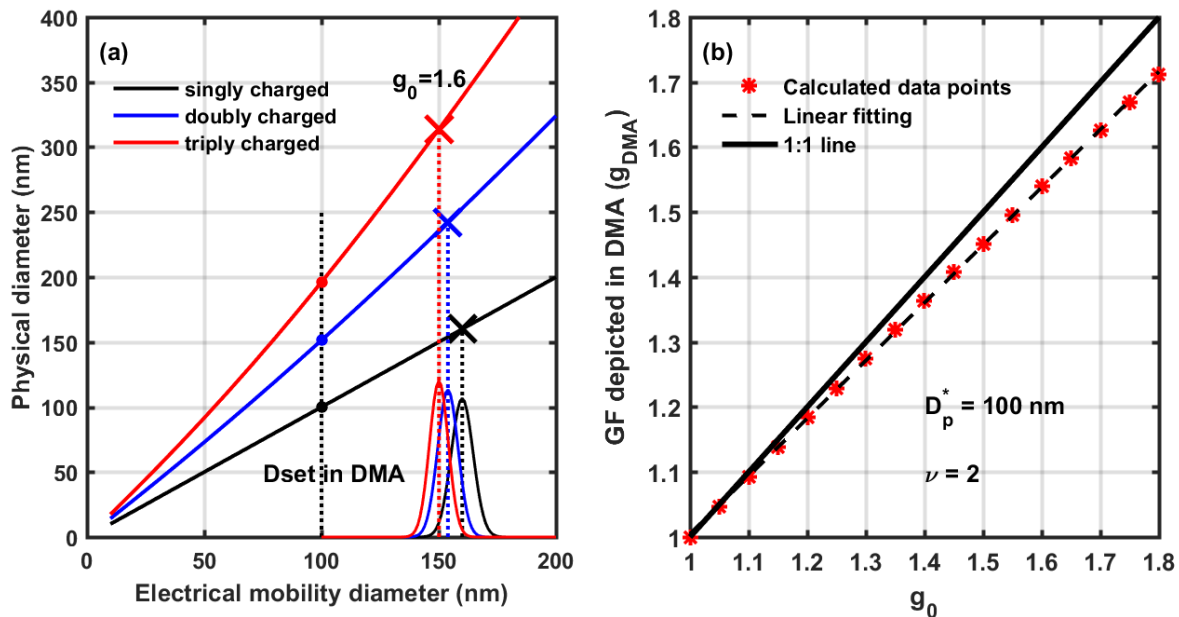
280 Table 1 The compression factor for aerosol particle's hygroscopicity under 85% RH over different electrical mobility diameters.

$\nu$ \ Dp (nm)	50	100	200	300	400	500	600
1	1	1	1	1	1	1	1
2	0.98	0.90	0.85	0.86	0.87	0.89	0.90
3	0.95	0.82	0.77	0.80	0.83	0.85	0.86
4	0.92	0.77	0.73	0.77	0.80	0.82	0.84
5	0.89	0.74	0.71	0.75	0.78	0.81	0.83



285 Figure 1. (a) Two cases of particle number size distribution during the field measurement. The black line represents the relatively clean period and the blue line represents the heavily polluted period. (b) The number ratio of particles carrying different charges. The left bar with black edge color corresponds to the PNSD in black line; the right bar without edge color corresponds to the PNSD in blue line.

290



295

Figure 2. (a) Effects of particle carrying multiple charges; black, blue and red lines represent singly, doubly and triply charges particles, respectively. The circle points are particles selected by DMA when the electrical mobility diameter is set as 100 nm. When the true growth factor is 1.6, these particles will grow to the corresponding crossed points. The mode of the MDF of multiply charged particles peaks at a smaller GF than the true value. (b) The compression effect of different growth factors for doubly charged particles with an electrical diameter of 100 nm.

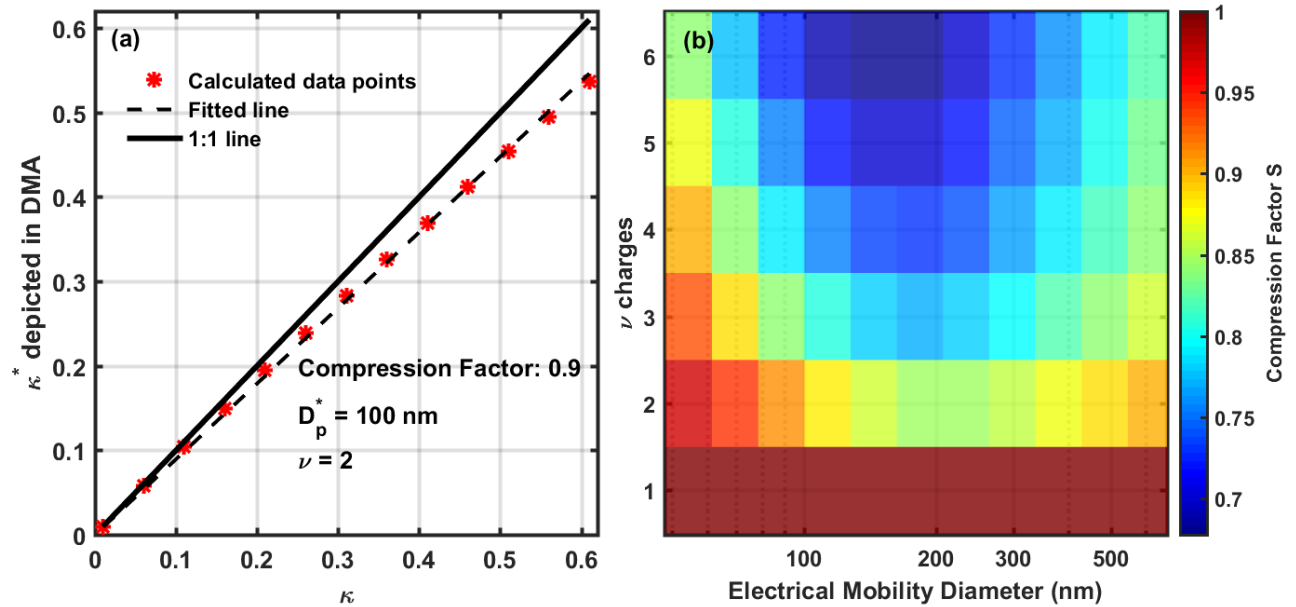


Figure 3. (a) The compression effect of different hygroscopicity (under 85% RH) for doubly charged particles with an electrical mobility diameter of 100 nm. The fitted slope or compression factor is 0.8953. (b) A summary of compression factors for different electrical mobility diameters carrying different number of charges at 85% RH.

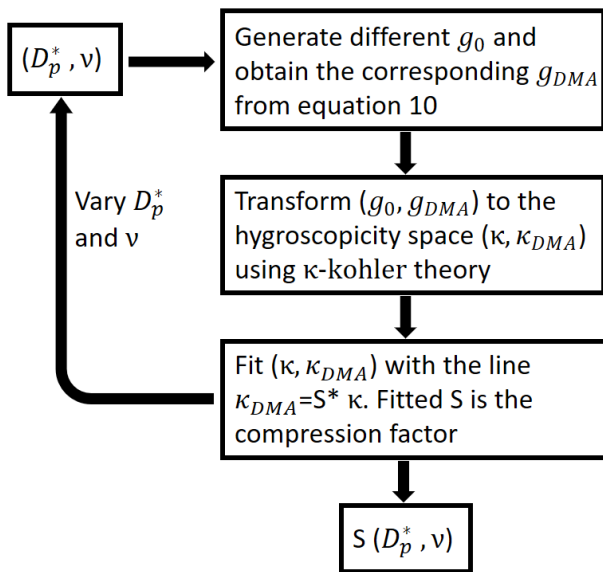
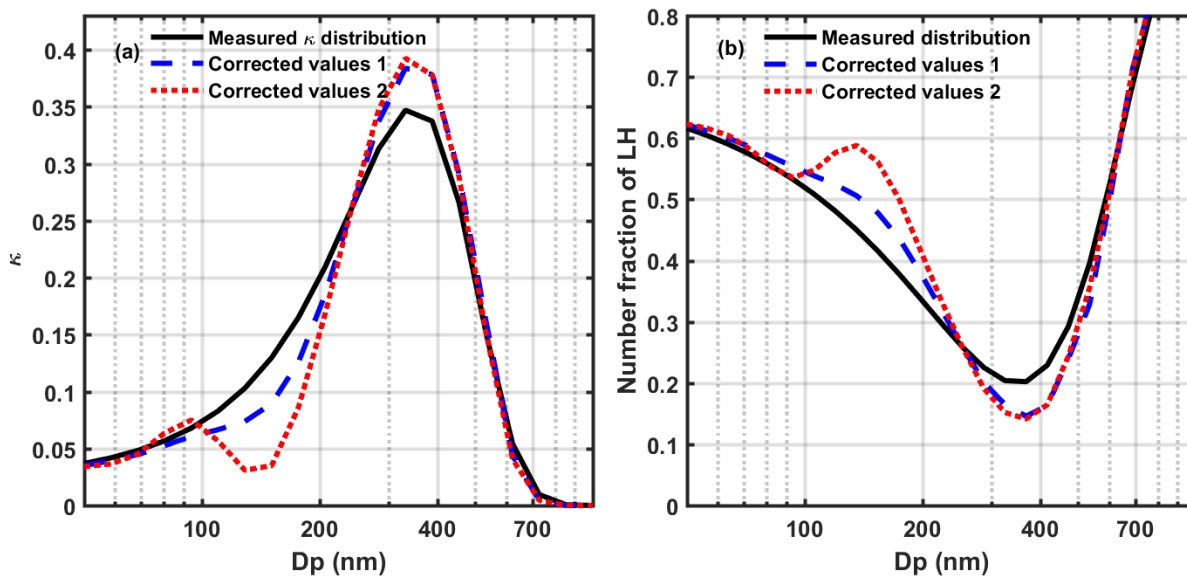


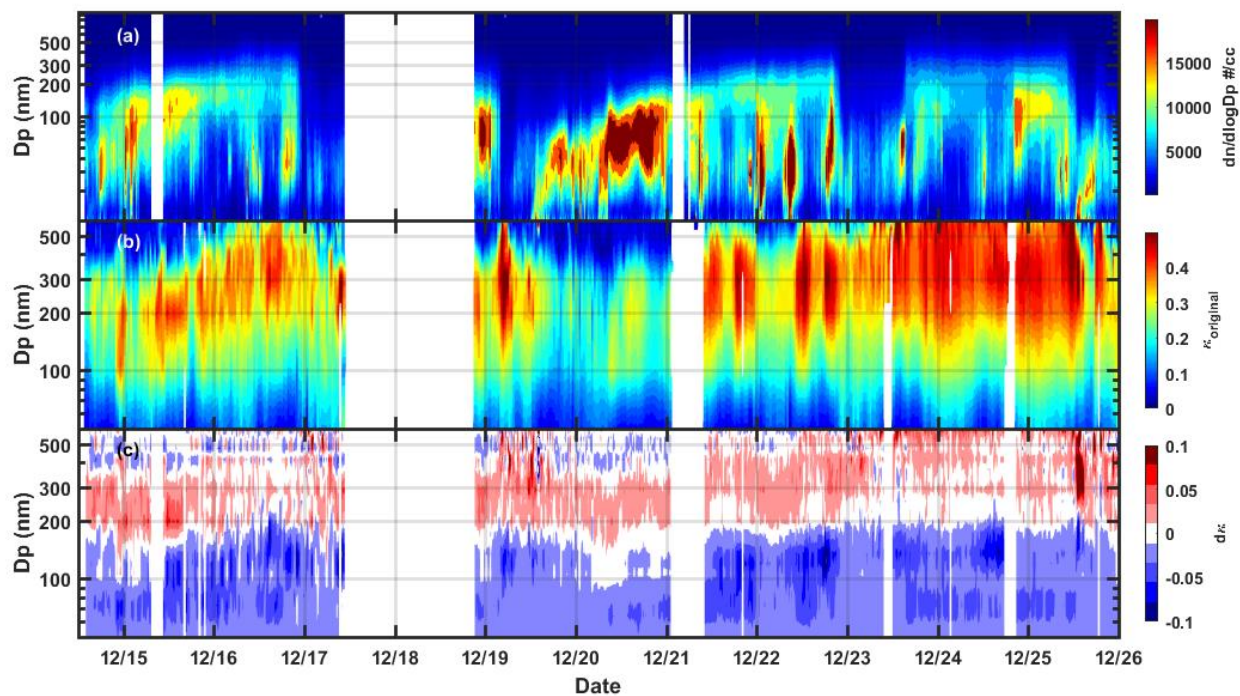
Figure 4. The algorithm procedures to calculate the compression factor.



310

Figure 5. (a) Multi-charge correction for one hypothetical measured  $\kappa$  distribution. The black line is the measured size-resolved  $\kappa$  and the dashed lines are the multi-charge corrected  $\kappa$  distributions based on different number size distributions. The used PNSD can be referred to in Fig. 1. (b) Multi-charge correction for one mixing state distribution. The black lines are the measured size-resolved number fraction of LH and the dashed lines are the multi-charge corrected values based on different number size distributions.

315



320 **Figure 6.** The field measurement of the PNSD and size-resolved hygroscopicity in Beijing winter. (a) The filled color gives the particle number concentration over different diameter ( $D_p$ ). (b) The filled color represents the size-resolved hygroscopicity parameter  $\kappa$ . (c) The difference between measured and multi-charge corrected  $\kappa$ .  $d_\kappa = \kappa_{corrected} - \kappa_{measured}$ .

## References

- 325 ALBRECHT, B. A.: Aerosols, Cloud Microphysics, and Fractional Cloudiness, *Science*, 245, 1227-1230, 10.1126/science.245.4923.1227, 1989.
- Bond, T. C., Doherty, S. J., Fahey, D. W., Forster, P. M., Berntsen, T., DeAngelo, B. J., Flanner, M. G., Ghan, S., Kärcher, B., Koch, D., Kinne, S., Kondo, Y., Quinn, P. K., Sarofim, M. C., Schultz, M. G., Schulz, M., Venkataraman, C., Zhang, H., Zhang, S., Bellouin, N., Guttikunda, S. K., Hopke, P. K., Jacobson, M. Z., Kaiser, J. W., Klimont, Z., Lohmann, U.,
- 330 Schwarz, J. P., Shindell, D., Storelvmo, T., Warren, S. G., and Zender, C. S.: Bounding the role of black carbon in the climate system: A scientific assessment, *Journal of Geophysical Research: Atmospheres*, 118, 5380-5552, 10.1002/jgrd.50171, 2013.
- CHARLSON, R. J., SCHWARTZ, S. E., HALES, J. M., CESS, R. D., COAKLEY, J. A., HANSEN, J. E., and HOFMANN, D. J.: Climate Forcing by Anthropogenic Aerosols, *Science*, 255, 423-430, 10.1126/science.255.5043.423, 1992.
- 335 Chen, J., Zhao, C. S., Ma, N., Liu, P. F., Göbel, T., Hallbauer, E., Deng, Z. Z., Ran, L., Xu, W. Y., Liang, Z., Liu, H. J., Yan, P., Zhou, X. J., and Wiedensohler, A.: A parameterization of low visibilities for hazy days in the North China Plain, *Atmospheric Chemistry and Physics*, 12, 4935-4950, 10.5194/acp-12-4935-2012, 2012.
- Cubison, M. J., Coe, H., and Gysel, M.: A modified hygroscopic tandem DMA and a data retrieval method based on optimal estimation, *J Aerosol Sci*, 36, 846-865, 10.1016/j.jaerosci.2004.11.009, 2005.
- 340 Deng, Z. Z., Zhao, C. S., Ma, N., Liu, P. F., Ran, L., Xu, W. Y., Chen, J., Liang, Z., Liang, S., Huang, M. Y., Ma, X. C., Zhang, Q., Quan, J. N., Yan, P., Henning, S., Mildenberger, K., Sommerhage, E., Schafer, M., Stratmann, F., and Wiedensohler, A.: Size-resolved and bulk activation properties of aerosols in the North China Plain, *Atmospheric Chemistry and Physics*, 11, 3835-3846, 10.5194/acp-11-3835-2011, 2011.
- Duplissy, J., Gysel, M., Alfarra, M. R., Dommen, J., Metzger, A., Prevot, A. S. H., Weingartner, E., Laaksonen, A.,
- 345 Raatikainen, T., Good, N., Turner, S. F., McFiggans, G., and Baltensperger, U.: Cloud forming potential of secondary organic aerosol under near atmospheric conditions, *Geophys Res Lett*, 35, 10.1029/2007gl031075, 2008.
- Ervens, B., Turpin, B. J., and Weber, R. J.: Secondary organic aerosol formation in cloud droplets and aqueous particles (aqSOA): a review of laboratory, field and model studies, *Atmospheric Chemistry and Physics*, 11, 11069-11102, 10.5194/acp-11-11069-2011, 2011.
- 350 Fierce, L., Onasch, T. B., Cappa, C. D., Mazzoleni, C., China, S., Bhandari, J., Davidovits, P., Fischer, D. A., Helgestad, T., Lambe, A. T., Sedlacek, A. J., 3rd, Smith, G. D., and Wolff, L.: Radiative absorption enhancements by black carbon controlled by particle-to-particle heterogeneity in composition, *Proc Natl Acad Sci U S A*, 117, 5196-5203, 10.1073/pnas.1919723117, 2020.
- Gysel, M., McFiggans, G. B., and Coe, H.: Inversion of tandem differential mobility analyser (TDMA) measurements, *J Aerosol Sci*, 40, 134-151, 10.1016/j.jaerosci.2008.07.013, 2009.
- 355 Haywood, J., and Boucher, O.: Estimates of the direct and indirect radiative forcing due to tropospheric aerosols: A review, *Reviews of Geophysics*, 38, 513-543, 10.1029/1999rg000078, 2000.
- Herrmann, H., Schaefer, T., Tilgner, A., Styler, S. A., Weller, C., Teich, M., and Otto, T.: Tropospheric aqueous-phase chemistry: kinetics, mechanisms, and its coupling to a changing gas phase, *Chem Rev*, 115, 4259-4334, 10.1021/cr500447k,
- 360 2015.
- Heyder, J., Gebhart, J., Rudolf, G., Schiller, C. F., and Stahlhofen, W.: Deposition of particles in the human respiratory tract in the size range 0.005–15  $\mu\text{m}$ , *J Aerosol Sci*, 17, 811-825, [https://doi.org/10.1016/0021-8502\(86\)90035-2](https://doi.org/10.1016/0021-8502(86)90035-2), 1986.
- Kreidenweis, S. M., and Asa-Awuku, A.: Aerosol Hygroscopicity: Particle Water Content and Its Role in Atmospheric Processes, 331-361, 10.1016/b978-0-08-095975-7.00418-6, 2014.
- 365 Ländahl, J., Massling, A., Pagels, J., Swietlicki, E., Vaclavik, E., and Loft, S.: Size-Resolved Respiratory-Tract Deposition of Fine and Ultrafine Hydrophobic and Hygroscopic Aerosol Particles During Rest and Exercise, *Inhalation Toxicology*, 19, 109-116, 10.1080/08958370601051677, 2007.
- McFiggans, G., Artaxo, P., Baltensperger, U., Coe, H., Facchini, M. C., Feingold, G., Fuzzi, S., Gysel, M., Laaksonen, A., Lohmann, U., Mentel, T. F., Murphy, D. M., O'Dowd, C. D., Snider, J. R., and Weingartner, E.: The effect of physical and
- 370 chemical aerosol properties on warm cloud droplet activation, *Atmos. Chem. Phys.*, 6, 2593-2649, 10.5194/acp-6-2593-2006, 2006.

- Petters, M., and Kreidenweis, S.: A single parameter representation of hygroscopic growth and cloud condensation nucleus activity, 2007.
- 375 Shen, C., Zhao, G., Zhao, W., Tian, P., and Zhao, C.: Measurement report: Aerosol hygroscopic properties extended to 600 nm in the urban environment, *Atmos. Chem. Phys. Discuss.*, 2020, 1-22, 10.5194/acp-2020-867, 2020.
- Stolzenburg, M. R., and McMurry, P. H.: Equations Governing Single and Tandem DMA Configurations and a New Lognormal Approximation to the Transfer Function, *Aerosol Science and Technology*, 42, 421-432, 10.1080/02786820802157823, 2008.
- 380 Swietlicki, E., Hansson, H. C., Hämeri, K., Svenningsson, B., Massling, A., McFiggans, G., McMurry, P. H., Pet ä ä T., Tunved, P., Gysel, M., Topping, D., Weingartner, E., Baltensperger, U., Rissler, J., Wiedensohler, A., and Kulmala, M.: Hygroscopic properties of submicrometer atmospheric aerosol particles measured with H-TDMA instruments in various environments—a review, *Tellus B: Chemical and Physical Meteorology*, 60, 432-469, 10.1111/j.1600-0889.2008.00350.x, 2008.
- 385 Swietlicki, E., Hansson, H. C., Hämeri, K., Svenningsson, B., Massling, A., McFiggans, G., McMurry, P. H., Pet ä ä T., Tunved, P., Gysel, M., Topping, D., Weingartner, E., Baltensperger, U., Rissler, J., Wiedensohler, A., and Kulmala, M.: Hygroscopic properties of submicrometer atmospheric aerosol particles measured with H-TDMA instruments in various environments—a review, *Tellus B: Chemical and Physical Meteorology*, 60, 432-469, 10.1111/j.1600-0889.2008.00350.x, 2017.
- 390 Tang, M., Chan, C. K., Li, Y. J., Su, H., Ma, Q., Wu, Z., Zhang, G., Wang, Z., Ge, M., Hu, M., He, H., and Wang, X.: A review of experimental techniques for aerosol hygroscopicity studies, *Atmospheric Chemistry and Physics*, 19, 12631-12686, 10.5194/acp-19-12631-2019, 2019.
- Twomey, S.: Pollution and the planetary albedo, *Atmospheric Environment* (1967), 8, 1251-1256, [http://dx.doi.org/10.1016/0004-6981\(74\)90004-3](http://dx.doi.org/10.1016/0004-6981(74)90004-3), 1974.
- 395 Voutilainen, A., Stratmann, F., and Kaipio, J. P.: A NON-HOMOGENEOUS REGULARIZATION METHOD FOR THE ESTIMATION OF NARROW AEROSOL SIZE DISTRIBUTIONS, *J Aerosol Sci*, 31, 1433-1445, [https://doi.org/10.1016/S0021-8502\(00\)00044-6](https://doi.org/10.1016/S0021-8502(00)00044-6), 2000.
- Wiedensohler, A., Lütke-meier, E., Feldpausch, M., and Helsper, C.: Investigation of the bipolar charge distribution at various gas conditions, *J Aerosol Sci*, 17, 413-416, [https://doi.org/10.1016/0021-8502\(86\)90118-7](https://doi.org/10.1016/0021-8502(86)90118-7), 1986.
- 400 Wu, Z., Wang, Y., Tan, T., Zhu, Y., Li, M., Shang, D., Wang, H., Lu, K., Guo, S., Zeng, L., and Zhang, Y.: Aerosol Liquid Water Driven by Anthropogenic Inorganic Salts: Implying Its Key Role in Haze Formation over the North China Plain, *Environmental Science & Technology Letters*, 5, 160-166, 10.1021/acs.estlett.8b00021, 2018.
- Xu, W., Kuang, Y., Bian, Y., Liu, L., Li, F., Wang, Y., Xue, B., Luo, B., Huang, S., Yuan, B., Zhao, P., and Shao, M.: Current Challenges in Visibility Improvement in Southern China, *Environmental Science & Technology Letters*, 7, 395-401, 10.1021/acs.estlett.0c00274, 2020.
- 405 Zhao, G., Tao, J., Kuang, Y., Shen, C., Yu, Y., and Zhao, C.: Role of black carbon mass size distribution in the direct aerosol radiative forcing, *Atmos. Chem. Phys.*, 19, 13175-13188, 10.5194/acp-19-13175-2019, 2019.